# Effect of pH on selective decomposition of target water contaminants onto porous $TiO_2$ photocatalyst

Abolfazl Zakersalehi and Hyeok Choi


## ABSTRACT

Non-selectivity of $TiO_2$-based photocatalysis is a known drawback of this technology for full scale water treatment applications. It results in significant decline in decomposition of toxic target contaminants when other non-toxic organic compounds such as natural organic matter (NOM) compete in the reaction. Previously, size exclusion of large NOM onto the mesoporous structure of $TiO_2$ photocatalyst was proven to improve the selective decomposition of small size target chemicals. In this study, manipulation of reaction pH as a crucial parameter in governing the adsorption and decomposition of organic chemicals was combined with the size exclusion of NOM. The effects of size-based adsorption/exclusion and pH-dependent electrostatic attraction/repulsion were investigated by using humic acid as model NOM and ibuprofen and methylene blue as model target contaminants. Adsorption and decomposition of the targets were dependent on their hydrodynamic size and ionization state. Mesoporous $TiO_2$ suppressed physical access of large NOM onto its surface while reaction pH influenced the surface charge of $TiO_2$ and the speciation of the chemicals and thus controlled their adsorption and decomposition. The results imply that selecting a proper pH can significantly improve selective decomposition of a target onto porous $TiO_2$ in the presence of NOM.


**Key words** | natural organic matter, reaction pH, selective decomposition, surface charge, $TiO_2$ photocatalysis, toxic contaminants

**Abolfazl Zakersalehi**
**Hyeok Choi** (corresponding author)
Department of Civil Engineering,
The University of Texas at Arlington,
Arlington,
TX 76019-0308,
USA
E-mail: *hchoi@uta.edu*

## INTRODUCTION

Decontamination of water resources using $TiO_2$ photocatalysis has been extensively studied. Currently, the process is typically applied in small scale water treatment while its full scale application is still challenging. The decomposition process is predominantly initiated by the generation of highly reactive oxidizing species such as hydroxyl radicals which can readily and non-selectively attack organic contaminants (Lazar & Daoud 2013). However, the non-selectivity of the process using hydroxyl radicals results in concurrent decomposition of many non-toxic (or less toxic) naturally abundant organic species such as natural organic matter (NOM), along with highly toxic target contaminants such as pharmaceuticals and dyes in water. This significantly declines the decomposition kinetics of target contaminants (Avisar *et al.* 2013). The issue becomes more critical considering that a relatively high concentration of NOM is present along with trace levels of highly toxic organic contaminants in water (Richardson & Ternes 2014). If possible with given effort, the decomposition process should focus more on toxic target chemicals than NOM although the decomposition of NOM as a known precursor of disinfection byproducts is also generally important.

Various physicochemical modifications of $TiO_2$ structure have been proposed to decompose only a target

doi: 10.2166/ws.2017.059

chemical or chemical group. Increasing the affinity of $TiO_2$ by surface grafting and modification, and incorporating $TiO_2$ into a porous material to initiate size-based separation have been reported to enhance the selectivity of $TiO_2$ photocatalysis (Yoneyama *et al.* 1989; Inumaru *et al.* 2004; Cropek *et al.* 2008). However, the previous studies requiring sophisticated technologies commonly demonstrated the introduction of a secondary material to $TiO_2$. In our effort to find an alternative solution, size exclusion of large NOM onto the mesoporous structure of $TiO_2$ photocatalyst was proven to be effective for the selective decomposition of small size targets (Zakersalehi *et al.* 2013). A narrow pore throat in the porous $TiO_2$ can act as a screen for retaining large size NOM while small target contaminants can freely enter the porous network. However, it is expected that even target chemicals experience slow mass transfer to such small pores, resulting in a decrease in overall reactivity.

As a result, a mechanistic tool to selectively attract target chemicals to the porous $TiO_2$ should be developed. Some studies demonstrated that changing overall reaction conditions can help to improve the selectivity (Bae *et al.* 2013; Yamamoto *et al.* 2013; Lu *et al.* 2015). In this study, the reaction pH as a crucial parameter in governing the adsorption and decomposition of such water contaminants was manipulated in combination with utilization of the porous $TiO_2$ for size exclusion of NOM. Electrostatic forces between $TiO_2$ and organic contaminants were triggered by changing the reaction pH (Suttiponparnit *et al.* 2011). Mechanistic studies on the effects of size-based exclusion and pH-dependent electrostatic force on the selective decomposition of target chemicals were carried out by using humic acid (HA) as model NOM and ibuprofen (IBP) and methylene blue (MB) as model target contaminants.

## MATERIALS AND METHODS

### Chemicals

IBP (Sigma-Aldrich) and MB (Sigma-Aldrich) were used without further purification. HA (Sigma-Aldrich) was pretreated to obtain a more uniform molecular size distribution. A cellulose membrane (molecular weight cut-off of 100,000 Da) in an Amicon Model 8200 (Millipore) ultrafiltration cell was used to filter out HA solution. The retained portion of HA on the membrane was re-suspended and used as model NOM in the photocatalytic experiment later. For synthesis of $TiO_2$, titanium tetraisopropoxide (TTIP, Sigma-Aldrich), polyoxyethylenesorbitan monooleate surfactant (Tween 80, Sigma-Aldrich), isopropanol (iPrOH, Sigma-Aldrich), and acetic acid (Sigma-Aldrich) were used without further purification.

### Synthesis and characterization

A surfactant-modified sol-gel method using an organic/inorganic sol was used for the synthesis of mesoporous $TiO_2$ (P-$TiO_2$), as described in detail elsewhere (Choi *et al.* 2006a; Zakersalehi *et al.* 2013). The sol was composed of Tween 80 as a pore templating agent, iPrOH as an organic solvent, acetic acid for the esterification reaction to generate water *in situ*, and TTIP as a $TiO_2$ precursor at a molar ratio of 2:45:6:1, respectively. Non-porous control $TiO_2$ (C-$TiO_2$) was also synthesized without the surfactant. After drying the sol for 24 h, the resulting gel was heat-treated at 500 °C in a programmable furnace (Paragon HT-22-D, Thermcraft) to remove the surfactant template and to transform to crystal phase $TiO_2$. $TiO_2$ particles were uniformly ground for further materials characterization and the photocatalytic experiment. The zeta potential of $TiO_2$ in aqueous dispersion at 0.5 g/L was measured by using a zeta potential analyzer (Horiba Z-100). The point of zero charge (PZC) of $TiO_2$ was also determined. The crystal structure of $TiO_2$ was examined by using X-ray diffraction (XRD) analysis employing a Kristalloflex D500 diffractometer (Siemens) with CuKa ($\lambda = 1.5406$ Å). The pore size distribution and surface area of $TiO_2$ was characterized by using a porosimetry analyzer (Tristar 3000, Micromeritics).

### Photocatalytic experiment and analysis

Photocatalytic decomposition of the target chemicals in the presence of NOM was tested to quantify the selectivity. Photocatalytic batch experiments were performed in a cylindrical open top glass container placed under two low pressure mercury ultraviolet (UV) lamps emitting 365 nm. UV intensity at the top of the reactor was measured at 3.1 mW/cm by using a photodiode laser measurement

sensor (PD-300RM-UV, Ophir Photonics). The volume of the reaction solution was 100 ml and $TiO_2$ concentration was 0.5 g/L. $TiO_2$ particles were dispersed by using a sonicator (Cole-Parmer 8891) prior to the experiment. Competitive conditions were constructed using HA, IBP, and MB at 17.9, 13.1, and 16.7 mg/L, respectively, which correspond to the same total organic carbon (TOC) concentration at 10 mg/L. Much higher concentrations of the target contaminants than their typical concentrations found in natural water at ppb and ppt levels were used in this study to avoid any analytical problems and limitations, in particular TOC measurement, as well as to quickly demonstrate the effect of pH on the selective decomposition without real-world complexity.

Phosphate buffer (Fluka) was used to control solution pH at 3–10. Samples were taken at 15 min intervals and were filtered by using a 0.45 μm syringe filter. The TOC of the chemicals was measured by using a TOC analyzer (Shimadzu TOC-Vcsn). The concentration of IBP was monitored by using a reversed-phase high performance liquid chromatograph (1200 series, Agilent) equipped with a UV detector at 214 nm while the concentration of MB was monitored by using a UV-visible spectrophotometer (Shimadzu UV-2550) at 590 nm. Maximum absorbance of IBP and MB was measured to be 214 nm and 590 nm, respectively which explains their negligible photolysis under the UV used in this study (365 nm), implying that the decomposition observed in this study later is mainly due to the photocatalytic reaction.

## RESULTS AND DISCUSSION

### $TiO_2$ surface charge over pH

Due to the amphoteric characteristics of $TiO_2$, precise control of reaction pH can be used to induce surface charge around $TiO_2$. The $TiO_2$ surface can undergo protonation below PZC and deprotonation above PZC, causing positive and negative surface charge, respectively. The electric potential and charge density are a function of several parameters including the crystalline properties of $TiO_2$ as well as the ionic strength of the reaction media (Preocanin & Kallay 2006). As shown in Figure 1, the zeta potential of P-$TiO_2$ and C-$TiO_2$ changed significantly over solution pH 3–11. Both C-$TiO_2$ and P-$TiO_2$ showed more or less similar behavior. Their PZCs were around pH 6.5. The highest zeta potential was observed around +45 mV at pH 3 and −40 mV at pH 11. Later, pH 6.5, 5, and 10 were used to represent neutral, acidic, and basic conditions, respectively, and thus to make the $TiO_2$ surface charged neutrally, positively, and negatively.

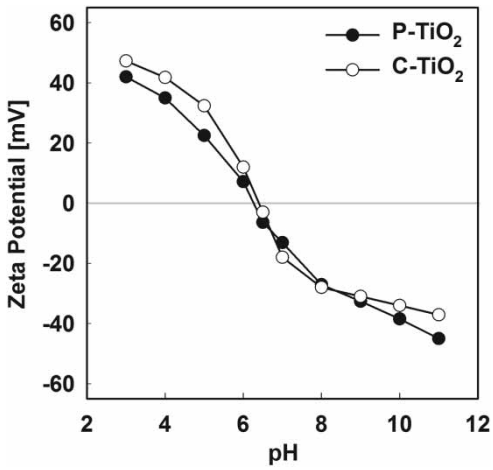


**Figure 1** | Effect of solution pH on zeta potential of aqueous $TiO_2$. PZC is the pH where the zeta potential of $TiO_2$ is zero.

### Structural properties of $TiO_2$ and size distribution of the chemicals

The XRD pattern of C-$TiO_2$ and P-$TiO_2$ is shown in Figure 2(a). They exhibited a strong diffraction peak at 25.4° indicative of the (101) lattice plane of the anatase crystal phase, which is known to be the most active for photocatalysis. As shown in Figure 2(b), P-$TiO_2$ exhibited distinct mesopore size distribution at 5–12 nm while C-$TiO_2$ did not show any apparent porous structure, indicating the significant role of the surfactant used as a pore directing agent in a $TiO_2$ inorganic matrix. Table 1 summarizes the physicochemical properties of C-$TiO_2$ and P-$TiO_2$. P-$TiO_2$ had a significantly higher surface area at 76.4 $m^2/g$ and porosity at 40.2% in comparison to surface area and porosity of C-$TiO_2$ at only 13.7 $m^2/g$ and 10.6%, respectively. The high surface area of P-$TiO_2$ originates from its internal porous structure, which might be less accessible for large size NOM.

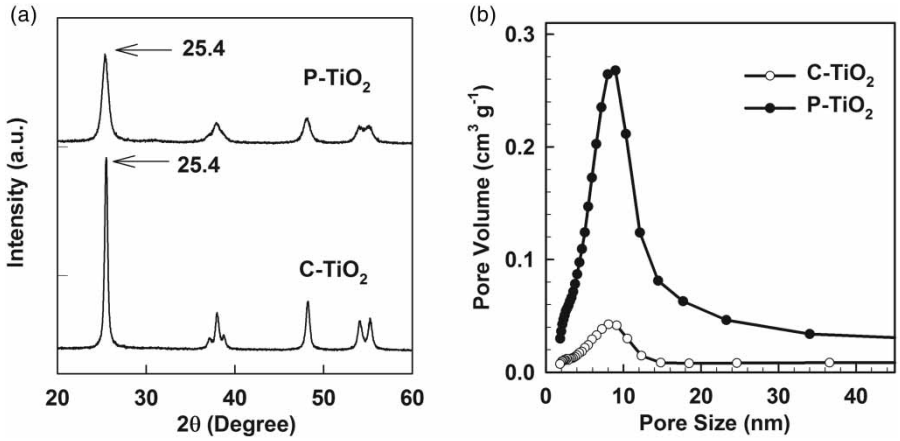


**Figure 2** | (a) XRD pattern and (b) pore size distribution of C-$TiO_2$ and P-$TiO_2$.

In comparison with the pore size of P-$TiO_2$ at 5–12 nm, the molecular size of the chemicals, IBP, MB, and HA, is shown in Figure 3. HA demonstrated an average hydrodynamic size of 8.1 nm, which is much larger than IBP at 1.0 nm and MB at 1.8 nm. The pores of P-$TiO_2$ are easily accessible for IBP and MB while they are less accessible for HA at 2–12 nm and thus HA might be size-excluded to a certain degree (not perfectly). It should be noted that synthesizing porous $TiO_2$ with smaller pores (e.g., 3–5 nm in this case) enough to exclude only HA effectively requires calcination of $TiO_2$ at a much lower temperature than 500 °C. However, such low temperatures generate poorly crystallized $TiO_2$ with an overall low reactivity (Choi *et al.* 2006b). The porous structure of P-$TiO_2$ is believed to significantly impact size exclusion of NOM as well as to provide plenty of catalytic sites for the chemicals for the photocatalytic reaction.

**Table 1** | Physicochemical properties of $TiO_2$ photocatalyst

| Parameter | C-$TiO_2$ | P-$TiO_2$ |
|---|---|---|
| Surface area[a] ($m^2$/g) | 13.7 | 76.4 |
| Pore volume ($cm^3$/g) | 0.028 | 0.159 |
| Porosity (%) | 10.6 | 40.2 |
| Pore diameter[b] (nm) | 7.38 | 7.31 |
| Crystal phase | Anatase | Anatase |
| Crystal size[c] | 16.3 | 11.6 |
| Porous nature | Control | Porous |

[a]Calculated based on Brunauer, Emmett, and Teller equation.
[b]Barrett, Joyner and Halenda adsorption pore diameter.
[c]Estimated based on Scherrer equation on the XRD peak.

## Adsorption of the organic chemicals

Considering the short lifetime of reactive hydroxyl radicals, success of $TiO_2$ photocatalysis is closely linked to availability of the organic chemicals adsorbing onto the active surface of $TiO_2$. The decomposition reaction also takes place through direct interaction of electrons or holes with surface-bounded contaminants. As proposed, the mesoporous structure of $TiO_2$ providing internal adsorption sites for mainly target contaminants and less likely for NOM can potentially increase the selective decomposition of the targets.

Figure 4 shows adsorption of IBP, MB, and HA onto C-$TiO_2$ and P-$TiO_2$ under dark conditions (no UV irradiation) at various pH conditions. In all cases, P-$TiO_2$ exhibited significantly higher adsorption capacity for IBP and MB than

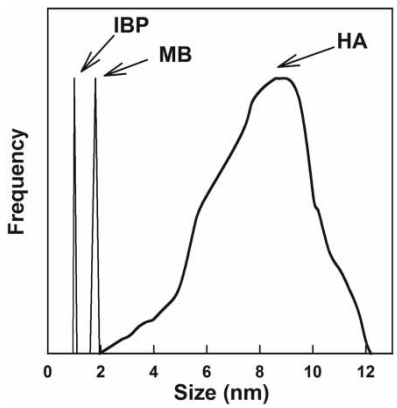


**Figure 3** | Relative molecular size distribution of IBP and MB (target chemicals) and HA (competing species).

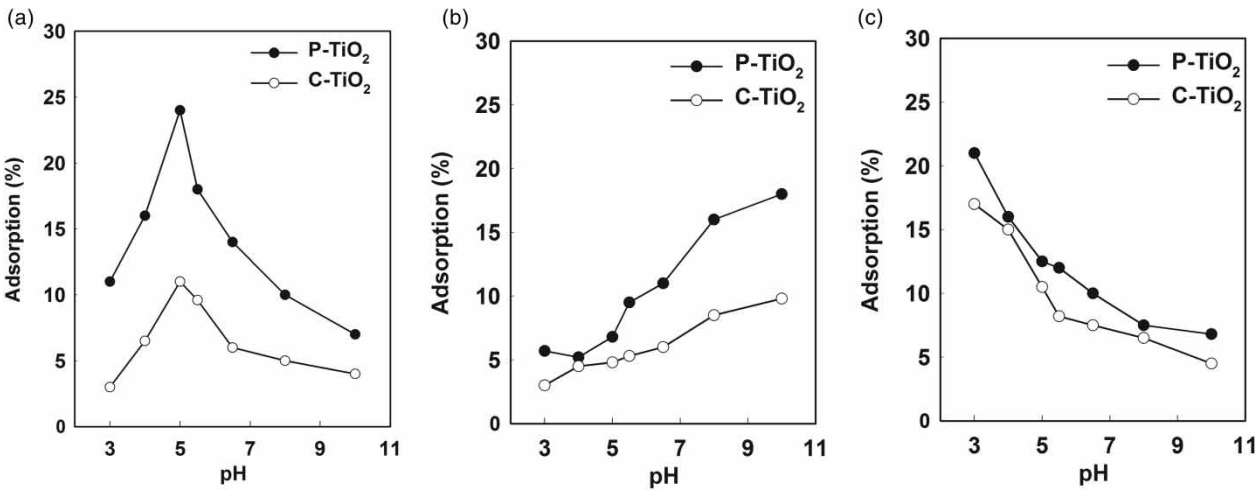


**Figure 4** | Dark condition adsorption of (a) IBP, (b) MB, and (c) HA onto C-$TiO_2$ and P-$TiO_2$ at various pH conditions.

C-$TiO_2$, which supports the hypothesis that the porous structure of P-$TiO_2$ can be easily utilized for adsorption of small size target chemicals. On the other hand, there was no significant difference in HA adsorption capacity between C-$TiO_2$ and P-$TiO_2$, implying that the inner porous structure of P-$TiO_2$, in spite of its high surface area, was less accessible for large size HA.

The highest adsorption of IBP occurred at around pH 5. With an increase in pH, adsorption of MB kept increasing while adsorption of HA kept decreasing. The pH dependency of adsorption of the chemicals can be partially explained by protonation/deprotonation of the $TiO_2$ surface (note Figure 1) and by its interaction with the charged chemicals over a range of pH values. IBP with a $pK_a$ of around 4.7 showed the highest adsorption at around pH 5 since a protonated $TiO_2$ surface (PZC of 6.5) can induce an attraction force for adsorption of mostly ionized IBP at this pH value (Domanska *et al.* 2009). Under acidic conditions of less than pH 5, most IBP molecules undergo protonation to form neutral molecules. Adsorption at this range is mainly governed by van der Waals force and hydrophobic interaction rather than electrostatic force. MB is strictly in cationic form under all the examined pH conditions and thus basic pH conditions favor adsorption of MB onto $TiO_2$ (Zhao *et al.* 2014). Adsorption of HA seems to follow anionic behavior in the pH range. Significant decrease in adsorption of HA at basic pH values could be explained by repulsion caused by the negatively charged $TiO_2$ surface and carboxylate ions around HA. With a decrease in pH, adsorption of HA continuously increased, along with an increase in the positive surface charge of $TiO_2$.

## Selective decomposition of IBP

Figure 5 shows adsorption and decomposition of IBP onto C-$TiO_2$ and P-$TiO_2$ at pH 5, 6.5, and 10 in the presence and absence of HA. Steeper IBP decomposition kinetic lines indicate overall higher reactivity while a smaller gap between the two IBP decomposition kinetic lines (i.e., IBP and IBP/HA) indicates better selectivity. In agreement with the previous adsorption results, P-$TiO_2$ demonstrated slightly more adsorption of IBP under dark conditions than C-$TiO_2$ at all the tested pH values. Both C-$TiO_2$ and P-$TiO_2$ showed high reactivity for decomposition of IBP in the absence of HA. The first order reaction rate constant at pH 5 was calculated at 0.037/min for C-$TiO_2$ and 0.043/min for P-$TiO_2$. The slightly higher rate constant for P-$TiO_2$ could be due to its higher surface area. The presence of HA in the reaction environment reduced the decomposition of IBP due to competition between IBP and HA for active sites on the $TiO_2$ surface and utilization of hydroxyl radicals. A much more significant decline in IBP decomposition kinetics was observed for C-$TiO_2$. Most of the surface of C-$TiO_2$ originates from its grain boundary (i.e., external surface) which both IBP and HA can access non-selectively.

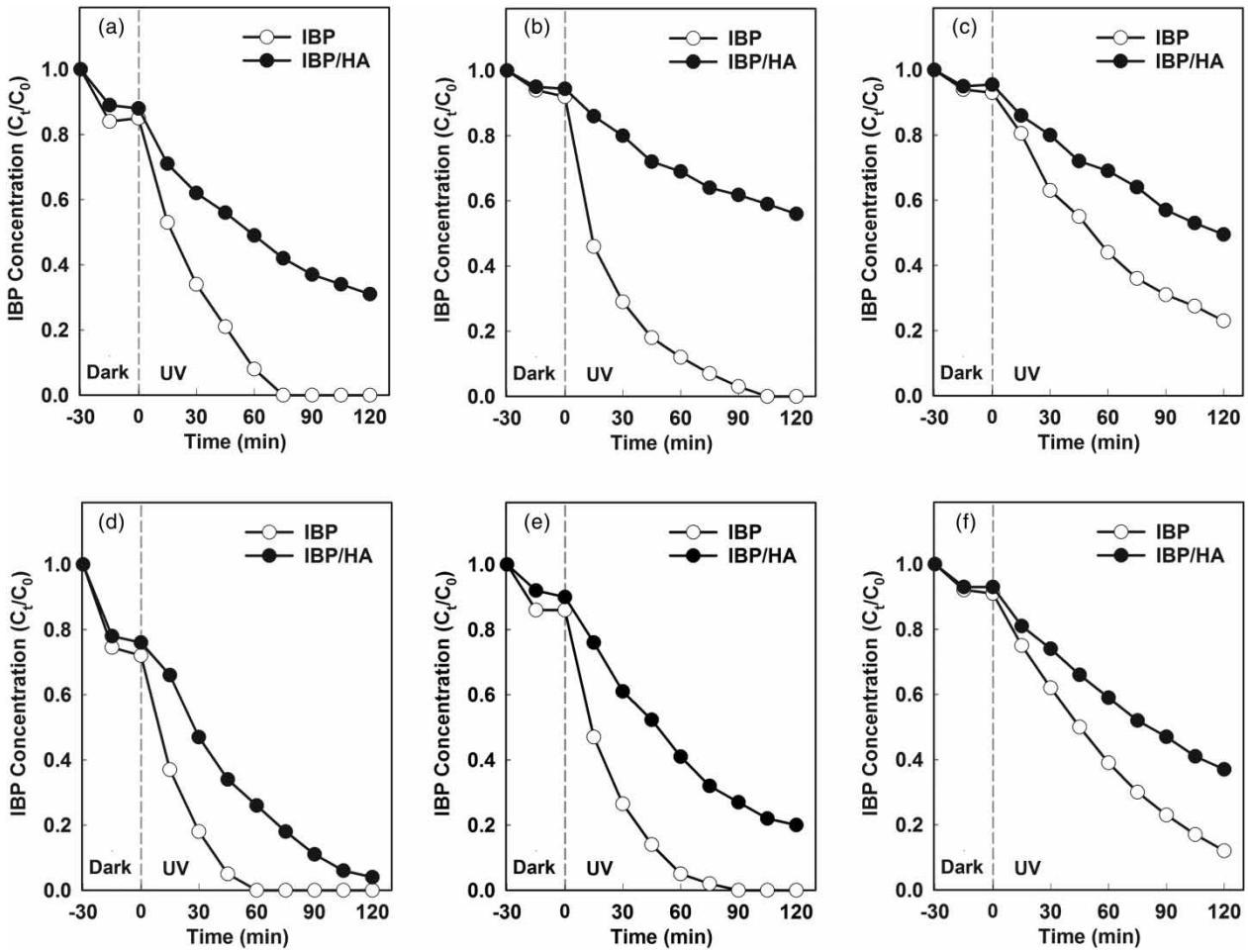


**Figure 5** | Photocatalytic decomposition of IBP onto (a) C-$TiO_2$ at pH 5, (b) C-$TiO_2$ at pH 6.5, (c) C-$TiO_2$ at pH 10, (d) P-$TiO_2$ at pH 5, (e) P-$TiO_2$ at pH 6.5, and (f) P-$TiO_2$ at pH 10 in the presence and absence of HA.

Meanwhile, there was much less decline in IBP decomposition kinetics on P-$TiO_2$ since its small inner pores were still available mainly for IBP decomposition. As observed in the previous adsorption test, changing the reaction pH to acidic conditions improved the reactivity of C-$TiO_2$ and P-$TiO_2$. At all the tested pH conditions, decomposition of IBP on P-$TiO_2$ was less affected by the presence of HA. Since both IBP and HA are in anionic form at the tested pH values, the selectivity enhancement was mainly due to HA size exclusion onto P-$TiO_2$. At all the conditions, P-$TiO_2$ demonstrated both higher reactivity and better selectivity towards IBP than C-$TiO_2$. The results supported the theory that both controlling the reaction pH at acidic conditions and leveraging size exclusion onto porous $TiO_2$ are beneficial for enhancing decomposition of IBP even in the presence of HA.

## Selective decomposition of MB

Figure 6 shows adsorption and decomposition of MB onto C-$TiO_2$ and P-$TiO_2$ at pH 5, 6.5, and 10 in the presence and absence of HA. Testing MB instead of IBP makes it possible to evaluate the effect of size exclusion combined with electrostatic forces because the experimental setup could investigate the effect of pH on selective decomposition of strictly cationic MB in the presence of mainly anionic HA onto P-$TiO_2$. Similarly to IBP, steeper MB decomposition kinetic lines indicate overall higher reactivity while a smaller gap between the two MB decomposition kinetic lines (i.e., MB and MB/HA) indicates better selectivity. General trends in MB decomposition were very similar to those in IBP decomposition, such as decomposition kinetic

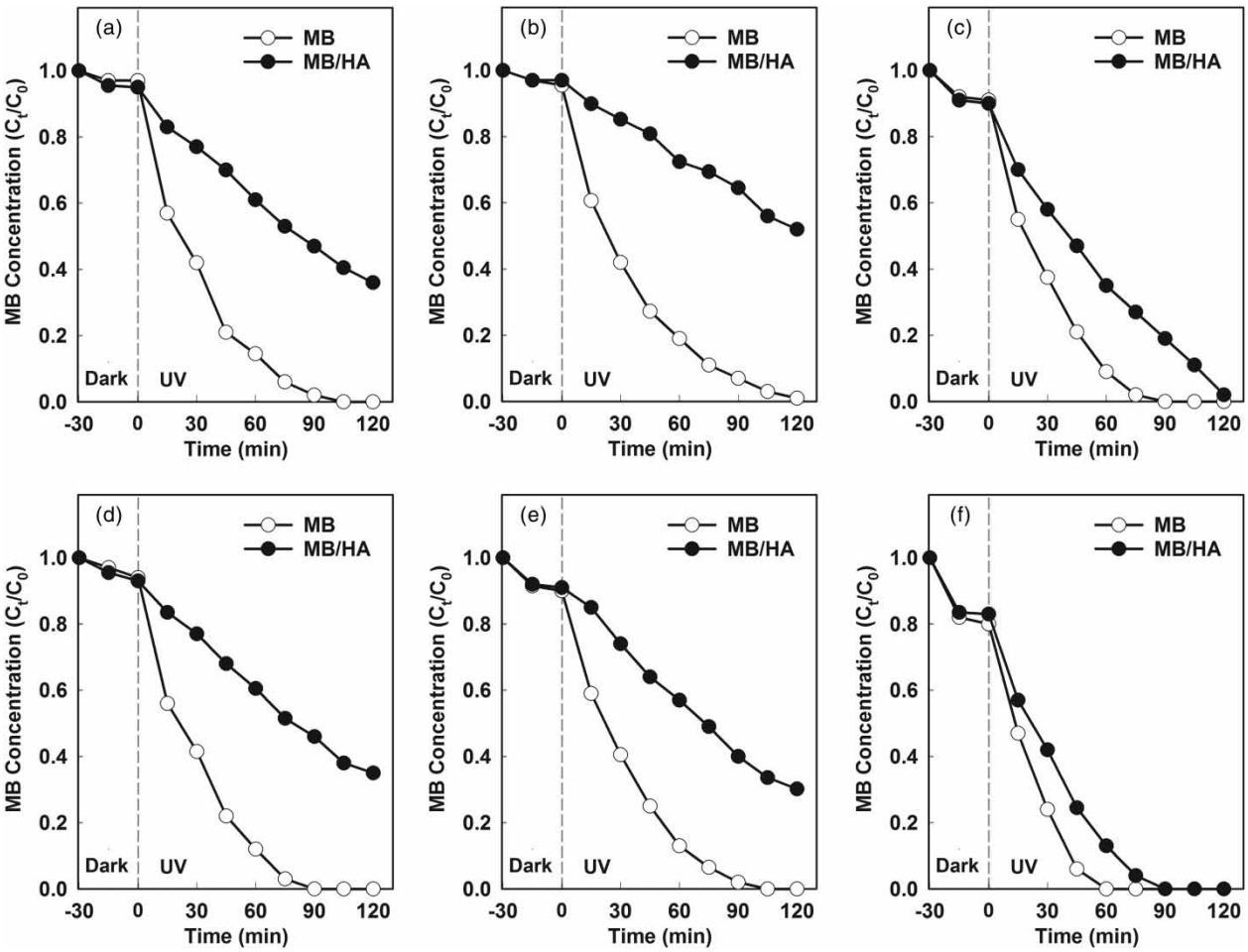


**Figure 6** | Photocatalytic decomposition of MB onto (a) C-$TiO_2$ at pH 5, (b) C-$TiO_2$ at pH 6.5, (c) C-$TiO_2$ at pH 10, (d) P-$TiO_2$ at pH 5, (e) P-$TiO_2$ at pH 6.5, and (f) P-$TiO_2$ at pH 10 in the presence and absence of HA.

decline in the presence of HA and higher reactivity of P-$TiO_2$ than C-$TiO_2$.

In general, the overall reactivity of C-$TiO_2$ and P-$TiO_2$ increased with increase in pH. Selective decomposition of MB was observed with P-$TiO_2$ more significantly at basic pH values. MB can be adsorbed more effectively onto P-$TiO_2$ due to the high surface area of P-$TiO_2$ and the attraction force between oppositely charged $TiO_2$ and MB at this pH condition. The presence of HA could not hinder the decomposition of MB due to the successful size exclusion of HA combined with the repulsive electrostatic force between negatively charged $TiO_2$ and anionic HA at the basic pH conditions. The selectivity which was observed even in the case of C-$TiO_2$ at pH 10 demonstrated well the role of the repulsive force between $TiO_2$ and HA. Meanwhile, the selectivity was weakened at acidic conditions because the $TiO_2$ surface has an attraction for adsorption of competing HA while MB adsorption is hindered. The results confirm the critical roles of NOM size exclusion onto porous $TiO_2$ and pH-dependent electrostatic forces in governing the photocatalytic decomposition of organic compounds.

## CONCLUSIONS

In an attempt to achieve the selective photocatalytic decomposition of toxic target water contaminants in the presence of less toxic NOM, the effect of reaction pH was studied. The results confirmed the critical roles of NOM size exclusion onto porous $TiO_2$ and pH-dependent

electrostatic forces between $TiO_2$ and organic chemicals in governing the selective photocatalytic decomposition of target chemicals. Both controlling the reaction pH (i.e., acidic condition for IBP and basic condition for MB) and leveraging the size exclusion could be beneficial for enhancing decomposition of a target contaminant even in the presence of NOM. Further investigations for real-world applications would include testing the approach with environmentally relevant concentrations of NOM and target chemicals, identifying possible complexation between NOM and co-existing common ionic species to form larger NOM, and eventually examining the approach with a real contaminated water matrix. Based on the presented results, engineering the porous structure of $TiO_2$ and changing the reaction pH appropriately can be used as a mechanistic tool to help the decomposition of target contaminants in the presence of NOM.

## ACKNOWLEDGEMENTS

The authors wish to thank the University of Texas at Arlington for financial support for this research.

## REFERENCES

Avisar, D., Horovitz, I., Lozzi, L., Ruggieri, F., Baker, M., Abeld, M. L. & Mamane, H. 2013 Impact of water quality on removal of carbamazepine in natural waters by N-doped $TiO_2$ photocatalytic thin film surfaces. *J. Hazard. Mater.* **244**, 463–471.

Bae, S., Jung, J. & Lee, W. 2013 The effect of pH and zwitterionic buffers on catalytic nitrate reduction by $TiO_2$-supported bimetallic catalyst. *Chem. Eng. J.* **232**, 327–337.

Choi, H., Stathatos, E. & Dionysiou, D. D. 2006a Synthesis of nanocrystalline photocatalytic $TiO_2$ thin films and particles using sol-gel method modified with nonionic surfactants. *Thin Solid Films* **510**, 107–114.

Choi, H., Kim, Y. J., Varma, R. S. & Dionysiou, D. D. 2006b Thermally stable nanocrystalline $TiO_2$ photocatalysts synthesized via sol-gel methods modified with ionic liquid and surfactant molecules. *Chem. Mater.* **18**, 5377–5384.

Cropek, D., Kemme, P. A., Makarova, O. V., Chen, L. X. & Rajh, T. 2008 Selective photocatalytic decomposition of nitrobenzene using surface modified $TiO_2$ nanoparticles. *J. Phy. Chem. C* **112**, 8311–8318.

Domanska, U., Pobudkowska, A., Pelczarska, A. & Gierycz, P. 2009 pKa and solubility of drugs in water, ethanol, and 1-octanol. *J. Phys. Chem. B* **113**, 8941–8947.

Inumaru, K., Murashima, M., Kasahara, T. & Yamanaka, S. 2004 Enhanced photocatalytic decomposition of 4-nonylphenol by surface-organografted $TiO_2$: a combination of molecular selective adsorption and photocatalysis. *Appl. Catal. B* **52**, 275–280.

Lazar, M. A. & Daoud, W. A. 2013 Achieving selectivity in $TiO_2$-based photocatalysis. *RSC Advances* **3**, 4130–4140.

Lu, X., Song, C., Jia, S., Tong, Z., Tang, X. & Teng, Y. 2015 Low-temperature selective catalytic reduction of NOX with $NH_3$ over cerium and manganese oxides supported on $TiO_2$–graphene. *Chem. Eng. J.* **260**, 776–784.

Preocanin, T. & Kallay, N. 2006 Point of zero charge and surface charge density of $TiO_2$ in aqueous electrolyte solution as obtained by potentiometric mass titration. *Croatica Chemica Acta* **79** (1), 95–106.

Richardson, S. D. & Ternes, T. A. 2014 Water analysis: emerging contaminants and current issues. *Analy. Chem.* **86** (6), 2813–2848.

Suttiponparnit, K., Jiang, J., Sahu, M., Suvachittanont, S., Charinpanitkul, T. & Biswas, P. 2011 Role of surface area, primary particle size, and crystal phase on titanium dioxide nanoparticle dispersion properties. *Nanoscale Res. Lett.* **6**, 1–27.

Yamamoto, A., Mizuno, Y., Teramura, K., Shishido, T. & Tanaka, T. 2013 Effects of reaction temperature on the photocatalytic activity of photo-SCR of NO with $NH_3$ over a $TiO_2$ photocatalyst. *Catal. Sci. Technol.* **3**, 1771–1775.

Yoneyama, H., Haga, S. & Yamanaka, S. 1989 Photocatalytic activities of microcrystalline $TiO_2$ incorporated in sheet silicates of clay. *J. Phy. Chem.* **93**, 4833–4837.

Zakersalehi, A., Nadagouda, M. & Choi, H. 2013 Suppressing NOM access to controlled porous $TiO_2$ particles enhances the decomposition of target water contaminants. *Catal. Comm.* **41**, 79–82.

Zhao, Z., Yuan, J., Fu, M., Su, L. & Li, Z. 2014 Removal of methylene blue from aqueous solution by using oil shale ash. *Oil Shale* **31** (2), 161–173.

First received 6 January 2017; accepted in revised form 22 March 2017. Available online 6 May 2017